Thermal and State-Selected Rate Constant Calculations for $O(^3P) + H_2 \rightarrow OH + H$ and Isotopic Analogs

Donald G. Truhlar

Department of Chemistry
University of Minnesota
Minneapolis, Minnesota 55455

Bruce C. Garrett
Chemical Dynamics Corporation
1550 West Henderson Road
Columbus, Ohio 43220

Abstract

We use ab initio potential energy surfaces, including new parametrizations of the bending potentials for the two lowest electronic states, to calculate the rate constants for the reaction $O(^3P) + H_2$. The dynamics calculations are based on variational transition state theory with multidimensional semiclassical tunneling corrections. We present results for the temperature range 250-2400K. In general the calculated rate constants for the thermal reaction are in excellent agreement with available experiments. We also calculate the enhancement effect for exciting H_2 to the first excited vibrational state. For the reaction of vibrationally excited H_2 the rate constant is based on a dynamical bottleneck of 7.2 kcal/mol, as compared to a saddle point value of 12.6 kcal/mol, and it is in good agreement with experiment. The good agreement of theory and experiment for the excited state rate provides a dramatic demonstration of the reality of dynamical bottlenecks at locations far from the saddle point.

1. Introduction

Theoretical advances in chemical kinetics often require integration of several kinds of information. The combination of electronic structure and chemical dynamics calculations provides one particularly fruitful way to gain a detailed understanding of the forces responsible for observed kinetic phenomena. In our own work we have made several calculations of chemical reaction rates based on potential energy surfaces derived in whole or in part on ab initio electronic structure theory. Systems studied have included the reactions $H + H_2$, $OH + H_2$, $O + OH$, $F + H_2$, and $O + H_2$.

The $O + H_2$ reaction, unlike all the others on the above list, has more than one low-lying potential energy surface. In addition to the $^1A'$ water surface, that does not correlate adiabatically to the ^3P state of O, there are two $^3A'$ surfaces and a $^3A''$ one that do. One $^3A'$ surface and the $^3A''$ surface form a degenerate Π state for all collinear goemetries but have different bend potentials: The $^3A''$ state has a significantly broader bending valley, and hence it dominates the thermal rate at most temperatures of interest, although the $^3A'$ state may make a non-negligible contribution at high temperature (1,2). The second $^3A'$ state is unimportant for the thermal reaction rate. In our previous calculations (3,4) we included only the contributions from reaction on the lowest-energy $^3A''$ surface. The collinear part of this surface was treated by the modified rotated Morse oscillator spline fit of Lee et al. (5) to the ab initio calculations of Walch et al. (1,2,6) and the bend potential was treated by an anti-Morse bend model (7-9) with one parameter adjusted to reproduce the harmonic bend potential at the saddle point for the same ab initio calculations. In the present paper we include both electronic states, and the potential energy surfaces are treated by an improved parametrization. The improved parametrization consists, for each of the two surfaces, of a three-parameter fit to the bend potential so that it agrees with the newest ab initio calculations (10)

for large-amplitude (45°) bends at three points along the reaction path, including both the saddle point and a point close to the vibrationally adiabatic ground-state barrier maximum. We use the PolCI calculations of Walch et al. (1,6,10) because (i) they are available at enough geometries to determine both potential energy surfaces in the regions important for the reaction rate and (ii) they appear reasonably accurate. We note that in our previous study (4) of the $O + H_2$ reaction, we calculated rate constants for five potential energy surfaces. Two of these, called surfaces P and M, were based on the PolCI calculations, and the results appeared to show that these were the most accurate of the five.

The procedure used to fit the bend potential in the present study is a specific example of a strategy that may be very useful in many cases (11), namely the fitting of a globally defined potential in the wide vicinity of a reaction path with special emphasis on dynamical bottleneck locations (12) as determined by variational transition state theory (13,14) or the adiabatic theory of reactions (15).

Having obtained a representation of the potential energy surface, we calculated both thermal rate constants and state-selected rate constants for vibrationally excited H_2 by variational transition state theory with semiclassical ground-state transmission coefficients (3,16-18). These methods have been shown to provide reasonably accurate estimates of the quantum mechanical local-equilibrium and state-selected reaction rates for most chemical reactions (3,13,14,19,20). In general we believe we can use these methods to calculate rate constants that are reliable for a given potential energy surface to within a factor of two or better at room temperature and above. This is sufficient to compare computed rate constants to experiment, to test ab initio potential energy surfaces, and to draw useful conclusions about which features of the potential energy surface are significant for determining the magnitudes of observed rate constants and kinetic isotope effects.

2. Potential Energy Surfaces

The $^3\Pi$ potential energy surface is represented by the rotated Morse oscillator spline function of Lee et al. (5) for collinear geometries augmented by an anti-Morse bend (AB) potential (7-9). The parameters of the bend potential are adjusted to ab initio calculations (1,6,10) in the region near the saddle point and the vibrationally adiabatic ground-state barrier maximum {the maximum of $V_a^G(s)$ in the notation used previously (12,17)}. Further details are given elsewhere (21).

3. Dynamical Calculations

We calculated a separate rate constant for each potential energy surface. Denoting these results by $k_{A''}$ and $k_{A'}$ respectively, the thermal (i.e., canonical ensemble) rate constant is

$$k = k_{A'} + k_{A''} \qquad 1)$$

Each of the single-surface rate constants includes a multiple-surface coefficient (22) equal to $3/Q_O^{el}$ where 3 is the electronic degeneracy of the generalized transition state and Q_O^{el} is the electronic partition function of atomic O.

The single-surface rate constants were calculated by improved canonical variational transition-state-theory (ICVT) with semiclassical ground-state transmission coefficients. The methods are described in detail elsewhere (3,16-18). First we calculate the minimum energy path (MEP) by following the negative gradient of the potential in mass-scaled coordinates. Then for each distance s along the MEP we calculate the improved generalized standard-state free energy of activation $\Delta G^{IGT,O}(T,s)$ for a generalized transition state at this s, where T is the temperature. The hybrid ICVT rate constant for temperature T is then given by

$$k^{ICVT}(T) = \min_s \frac{\tilde{k}T}{h} K^{\neq,0} \exp[-\Delta G^{IGT,0}(T,s)/\tilde{k}T] \qquad 2)$$

where $\tilde{k}$ is Boltzmann's constant, h is Planck's constant, and K^0 is the reciprocal of the standard-state concentration. This rate constant is a hybrid because the reaction coordinate is treated classically but other degrees of freedom are all treated quantally. In the final step we add quantal effects on the reaction coordinate by a ground-state (G) transmission coefficient $\kappa^G(T)$:

$$k^{ICVT/G}(T) = \kappa^G(T) k^{ICVT}(T) \qquad 3)$$

We consider two methods to approximate $\kappa^G(T)$: the minimum-energy-path semiclassical adiabatic method (MEPSAG) (17) and the least-action method (LAG)(18). The latter accounts for the shortening of the tunneling path due to the system "cutting the corner" of the curved MEP through mass-scaled coordinates by finding the dynamically optimal tunneling path by evaluating an imaginary-action functional along a one-parameter sequence of trial paths. These vary linearly between the MEP at one extreme and a straight line through mass-scaled coordinates from the translational turning point on the MEP in the entrance channel to the translational turning point on the MEP in the exit channel at the other extreme.

Anharmonicity is included as discussed elsewhere (3,17).

The evaluation of state-selected rate constants for H_2 in the n=1 excited vibrational state requires further assumptions. Figure 1 shows the vibrationally adiabatic potential curves for n=0 and 1 for the $^3A''$ surface. The potential curves in Fig. 1 are defined by

$$V_a^g(n,s) = V_{MEP}(s) + \varepsilon_{str}(n,s) + 2\varepsilon_{bend}^g(s) \qquad 4)$$

where $V_{MEP}(s)$ is the Born-Oppenheimer potential on the MEP, $\varepsilon_{str}(n,s)$ is the local vibrational energy of the stretching mode orthogonal to the MEP and in quantum state n, and $2\varepsilon_{bend}^g(s)$ is the local zero point energy of the twofold-degenerate bending mode. Figure 2 shows the same quantities for the $^3A'$ state. In both cases we also show the curvature $\kappa(s)$ of the MEP through mass-scaled coordinates (17). We will consider two limits for the excited-state rate constants. The first is the adiabatic limit (4,16,18,23), in which case we perform calculations identical to those for the thermal reaction rate except that in both $\Delta G^{IGT,0}(T,s)$ and the tunneling calculation we neglect all stretching vibrational states except the n=1 state. The second treatment is a sudden nonadiabatic model explained elsewhere (21).

We will consider three reactions:

$$O + H_2 \rightarrow OH + H \qquad R1)$$

$$O + D_2 \rightarrow OD + D \qquad R2)$$

$$O + HD \rightarrow OH + D \text{ and } OD + H \qquad R3)$$

4. Results

Table I shows results for two methods of calculating transmission coefficients. The MEPSAG results are based on a semiclassical adiabatic treatment of tunneling along the minimum energy path (17). As compared to the LAG method this underestimates the rate constrant by a factor of 24 at 200K and a factor of 3.3 at 300K. This

confirms, as first discovered for the $H + H_2$ reaction (24) and then found in many cases (4,13,16-19,25-31), that multidimensional effects on the tunneling probabilities are very important and reduction to a one-dimensional problem by simply straightening out the minimum-energy reaction path seriously underestimates the extent of tunneling.

Table I also compares the final thermal rate constants of this study for reaction R1) to a selection of experimental (32-34) results. For 297-472K, the table shows only the most recent experimental data (32). The ICVT/LAG rate constants are usually larger than these results but agree within 25%. Rate constants in this temperature range are very sensitive to the barrier height, and the uncertainty in the *ab initio* potential energy surface is certainly great enough to yield larger errors. Thus the agreement of the present calculations with experiment is better than could have been expected. Furthermore the other recent experimental measurements in this range do not all agree with those of Presser and Gordon within a factor of two. The most recent evaluation (33) of experimental data for the $O + H_2$ reaction concludes that for $T \geq 400K$ the expression of Baulch *et al.* (34) fits most of the data within experimental error. We use this expression for the experimental values at 600-1500K. In this temperature range the present calculated rate constants are all larger than these experimental results, but the ICVT/LAG results are high only by factors of 1.2-1.5. At 2400K the agreement with experiment (35) is excellent.

We also calculated thermal rate coefficients for the isotopic analog reactions and the kinetic isotope effects and compared them to experimental (32,34-37) results. Because of space limitations we simply point out here that the calculated results agree with the experimental ones within the reliability of the latter. We also calculated kinetic isotope effects by conventional transition state theory (TST). These are qualitatively similar to the ICVT/LAG results, and hence also to the experimental results, but that is at least partly fortuitous since TST greatly underestimates the individual isotopic rate constants. For example for reaction R1) the TST rate constant is a factor of 9.3 lower than the ICVT/LAG one at 300K and a factor of 2.5 smaller at 400K. The LAG transmission coefficients are even larger, 12.6 at 300K and 3.1 at 400K, but the lack of quantal effects on reaction-coordinate motion in conventional TST is partly compensated by the lack of variational minimization of the hybrid rate constant with respect to the location of the generalized transition state. Then a further cancellation of errors occurs in the kinetic isotope effect ratio.

The adiabatic and sudden nonadiabatic rate constants for reaction R1) with vibrationally excited H_2 are very similar for the present potential energy surface; thus we tabulate only the adiabatic values. The rate constants calculated by the adiabatic theory for reaction R1) when H_2 is excited to the n=1 vibrational state are given in Table II. We see that the transmission coefficients (ratios of ICVT/LAG tunneling-corrected rate constants to ICVT hybrid ones) are 2.6-2.7 at 302K, which are very significant factors but are smaller than for the thermal reaction rate. At 302K the calculated vibrational enhancement factor in the ICVT/LAG approximation is 1.4×10^3 by Light (38), but it is only 8.2×10^2 times larger than the interpolated vaule of Presser and Gordon (32). The agreement of theory with experiment is satisfactory.

Table III shows some of the properties of the dynamical bottlenecks for the vibrationally excited reaction. The variational transition states are farther from the saddle point (s=0) for the vibrationally excited reaction than for the thermal reaction. Similar results have been found previously for $H + H_2$ (23) and $OH + H_2$ (39) for vibrationally excited reactants. This means that the improved parametrization of the bend potential for geometries far from the saddle point becomes more important for n=1. It also means that conventional TST becomes worse. Conventional TST predicts a vibrational enhancement factor of 2.5×10^5 at 302K, which is two orders larger than the accurate values. The good agreement of the ICVT/LAG values with experiment provides a dramatic demonstration of the reality of dynamical bottlenecks at locations far from the saddle point.

5. Acknowledgments

The authors are grateful to A. F. Wagner for helpful correspondence. The work at the University of Minnesota was supported in part by the U.S. Department of Energy, Office of Basic Energy Sciences, under contract no. DE-AC02-79ER10425 and that at Chemical Dynamics Corporation was supported in part by the Army Research Office through contract no. DAAG-29-84-C-0011.

TABLE I. Thermal rate constants ($cm^3 molecule^{-1} s^{-1}$) for $O + H_2 \rightarrow OH + H$.

T(K)	ICVT	ICVT/MEPSAG	ICVT/LAG	Exp.
250	2.94(-20)	2.35(-19)	1.77(-18)	...
297	8.45(-19)	3.32(-18)	1.15(-17)	1.0(-17)[a]
318	2.76(-18)	8.85(-18)	2.38(-17)	1.9(-17)[a]
370	2.93(-17)	6.66(-17)	1.20(-16)	1.1(-16)[a]
422	1.75(-16)	3.24(-16)	4.70(-16)	3.8(-16)[a]
472	6.84(-16)	1.10(-15)	1.43(-15)	1.2(-15)[a]
600	8.21(-15)	1.09(-14)	1.24(-14)	1.0(-14)[b]
1000	3.89(-13)	4.28(-13)	4.45(-13)	3.4(-13)[b]
1500	3.31(-12)	3.43(-12)	3.52(-12)	2.3(-12)[b]
2400	2.10(-11)	2.07(-11)	2.15(-11)	2.1(-11)[c]

[a] Presser and Gordon (32).

[b] Baulch *et al.* (34).

[c] Pamidimukkala and Skinner (35).

TABLE II. Rate constants ($cm^3 molecule^{-1} s^{-1}$) for the state-selected reaction $O + H_2(n=1) \rightarrow OH + H$.

T(K)	ICVT	ICVT/LAG	Exp.[a]
250	1.03(-15)	4.25(-15)	...
302	7.31(-15)	1.89(-14)	1.0(-14)
400	7.68(-14)	1.31(-13)	...
1000	8.58(-12)	9.33(-12)	...
2400	7.73(-11)	7.84(-11)	...

[a] from Light (38).

TABLE III. Bottleneck properties at conventional and canonical variational transition states for $O + H_2(n=1) \rightarrow OH + H$.[a]

Surface	T (K)	s (a_0)	r_{12} (a_0)	r_{23} (a_0)	V_{MEP} (kcal/mol)	$V_a^g(n=1)$ (kcal/mol)	$\epsilon_{str}(n=1)$ (kcal/mol)	$2\epsilon_{bend}^g$ (kcal/mol)
$^3A''$	...	0.00	2.29	1.74	12.58	19.07	4.89	1.61
	300	-0.55	2.95	1.45	7.22	23.02	14.74	1.07
	1000	-0.51	2.91	1.45	7.64	22.96	14.22	1.10
$^3A'$	...	0.00	2.29	1.74	12.58	20.00	4.89	2.53
	300	-0.54	2.93	1.45	7.36	23.92	14.57	1.98
	1000	-0.51	2.90	1.45	7.69	23.87	14.14	2.04

[a] r_{12} and r_{23} are the nearest-neighbor OH and HH distances at the saddle point (s=0) or the variational transition state for the temperature indicated. 1 a_0 = 1 bohr = 0.5292 Å.

References

(1) S. P. Walch, A. F. Wagner, T. H. Dunning, Jr., and G. C. Schatz, J. Chem. Phys. 72, 2894 (1980).

(2) T. H. Dunning, Jr., S. P. Walch, and A. F. Wagner, in Potential Energy Surfaces and Dynamics Calculations, edited by D. G. Truhlar (Plenum Press, New York, 1981), p. 329.

(3) B. C. Garrett and D. G. Truhlar, J. Chem. Phys. 81, 309 (1984).

(4) D. G. Truhlar, K. Runge, and B. C. Garrett, in Proc. Twentieth Int. Symp. Combustion (Combustion Institute, Pittsburgh), p. 585.

(5) K. T. Lee, J. M. Bowman, A. F. Wagner, and G. C. Schatz, J. Chem. Phys. 76, 3563 (1982).

(6) S. P. Walch, T. H. Dunning Jr., F. W. Bobrowicz, and R. Raffenetti, J. Chem. Phys. 72, 406 (1980).

(7) H. S. Johnston, Gas Phase Reaction Rate Theory (Ronald Press, New York, 1966).

(8) B. C. Garrett and D. G. Truhlar, J. Am. Chem. Soc. 101, 4534 (1979).

(9) B. C. Garrett, D. G. Truhlar, and A. W. Magnuson, J. Chem. Phys. 76, 2321 (1982).

(10) J. M. Bowman, A. F. Wagner, S. P. Walch, and T. H. Dunning, Jr., J. Chem. Phys. 81, 1739 (1984).

(11) D. G. Truhlar, F. B. Brown, R. Steckler, and A. D. Isaacson, in Proceedings of the NATO/CECAM Workshop on Theory of Chemical Reaction Dynamics, Orsay, France, June 1985.

(12) B. C. Garrett, D. G. Truhlar, and R. S. Grev, in Potential Energy Surfaces and Dynamics Calculations, edited by D. G. Truhlar (Plenum Press, New York, 1981), p. 587.

(13) D. G. Truhlar and B. C. Garrett, Acc. Chem. Res. 13, 440 (1980).

(14) D. G. Truhlar and B. C. Garrett, Annu. Rev. Phys. Chem. 35, 159 (1984).

(15) D. G. Truhlar, J. Chem. Phys. 53, 2041 (1970).

(16) B. C. Garrett and D. G. Truhlar, J. Phys. Chem. 83, 1079 (1979), errata: 84, 682 (1980), 87, 4553 (1983).

(17) B. C. Garrett, D. G. Truhlar, R. S. Grev, and A. W. Magnuson, J. Phys. Chem. 84, 1730 (1980); errata: 87, 4554 (1983).

(18) B. C. Garrett and D. G. Truhlar, J. Chem. Phys. 79, 4931 (1983).

(19) D. G. Truhlar, A. D. Isaacson, R. T. Skodje, and B. C. Garrett, J. Phys. Chem. 86, 2252 (1982); errata: 87, 4554 (1983).

(20) D. G. Truhlar, W. L. Hase, and J. T. Hynes, J. Phys. Chem. 87, 2664 (1983); errata: 87, 5523 (1983).

(21) B. C. Garrett and D. G. Truhlar, Int. J. Quantum Chem., to be published.

(22) D. G. Truhlar, J. Chem. Phys. 56, 3189 (1972), 61, 440(E) (1974).

(23) B. C. Garrett and D. G. Truhlar, J. Phys. Chem. 89, 2204 (1985).

(24) D. G. Truhlar and A. Kuppermann, Chem. Phys. Lett. 9, 269 (1971).

(25) R. A. Marcus and M. E. Coltrin, J. Chem. Phys. 67, 2609 (1977).

(26) B. C. Garrett and D. G. Truhlar, J. Chem. Phys. 72, 3460 (1980).

(27) B. C. Garrett, D. G. Truhlar, R. S. Grev, and R. B. Walker, J. Chem. Phys. 73, 235 (1980).

(28) D. K. Bondi, D. C. Clary, J. N. L. Connor, B. C. Garrett, and D. G. Truhlar, J. Chem. Phys. 76, 4986 (1982).

(29) R. T. Skodje, D. G. Truhlar, and B. C. Garrett, J. Chem. Phys. 77, 5955 (1982).

(30) D. K. Bondi, J. N. L. Connor, B. C. Garrett, and D. G. Truhlar, J. Chem. Phys. 78, 5981 (1983).

(31) A. D. Isaacson, M. T. Sund, S. N. Rai, and D. G. Truhlar, J. Chem. Phys. 82, 1338 (1985).

(32) N. Presser and R. J. Gordon, J. Chem. Phys. 82, 1291 (1985).

(33) N. Cohen and K. Westberg, J. Phys. Chem. Ref. Data 12, 531 (1983).

(34) D. L. Baulch, D. D. Drysdale, D. G. Horne, and A. C. Lloyd, Evaluated Kinetic Data for High-Temperature Reaction, Vol. 1 (Butterworths, London, 1972), p. 49.

(35) K. M. Pamidimukkala and G. B. Skinner, J. Chem. Phys. 76, 311 (1982).

(36) A. Westenberg and N. deHaas, J. Chem. Phys. 47, 4241 (1967).

(37) A. Westenberg and N. deHaas, J. Chem. Phys. 50, 2512 (1969).

(38) G. C. Light, J. Chem. Phys. 68, 2831 (1978).

(39) D. G. Truhlar and A. D. Isaacson, J. Chem. Phys. 77, 3516 (1982).

Figure captions

Fig. 1. Vibrationally adiabatic potential curves (solid curves with scale at left) defined by eq. 4) for n=0 and 1 and curvature of the reaction path (dashed curve with scale at right) as functions of the distance s along the minimum energy path through mass-scaled coordinates for the $^3A''$ potential energy surface. The saddle point is at s=0. The long tick marks on the ordinate scales denote the energies of $O + H_2(n=1)$, left side, and $OH(n=1) + H$, right side.

Fig. 2. Same as Fig. 1 except for $^3A'$ surface.

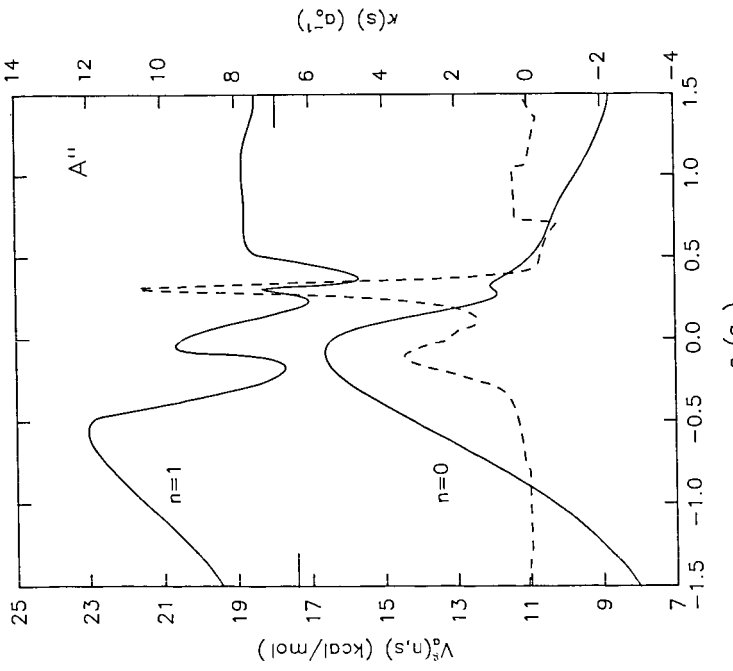

Fig. 1. Vibrationally adiabatic potential curves (solid curves with scale at left) defined by eq. 4) for n=0 and 1 and curvature of the reaction path (dashed curve with scale at right) as functions of the distance s along the minimum energy path through mass-scaled coordinates for the $^3A''$ potential energy surface. The saddle point is at s=0. The long tick marks on the ordinate scales denote the energies of $O + H_2(n=1)$, left side, and $OH(n=1) + H$, right side.

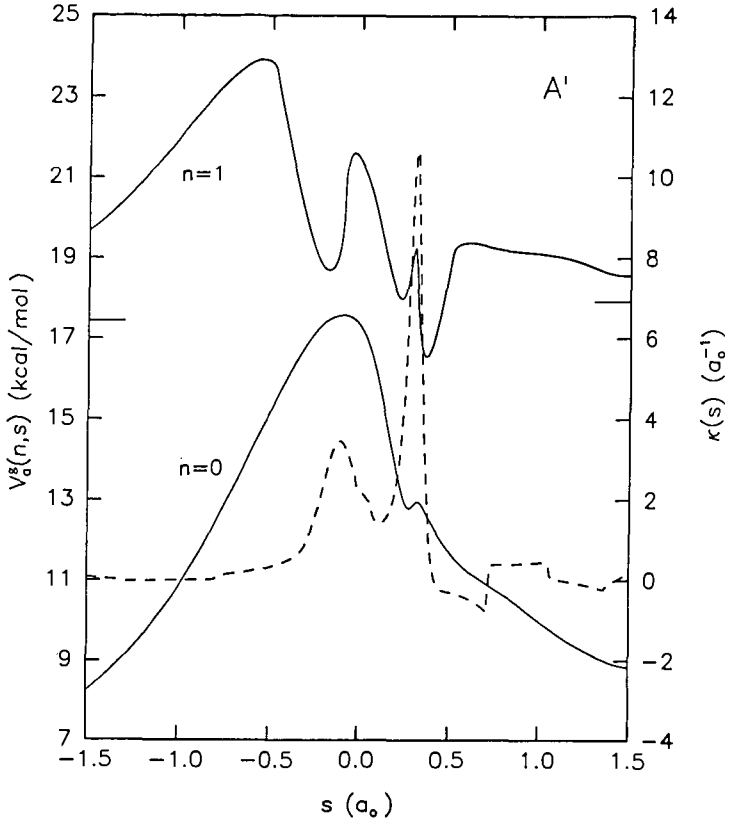

Fig. 2. Same as Fig. 1 except for $^3A'$ surface.